pp 1187–1199. © Royal Aeronautical Society 2017
doi: 10.1017/aer.2017.48

Experimental investigation of the onset of sand deposits on Hastelloy-X between 1,000°C and 1,100°C

A. Boulanger
aboulang@vt.edu

J. Hutchinson, W.F. Ng and S.V. Ekkad
Virginia Tech
College of Engineering, Department of Mechanical Engineering
Blacksburg, Virginia
US

M.J. Keefe and W. Xu
Virginia Tech
College of Science, Department of Statistics
Blacksburg, Virginia
US

B. Barker and K. Hsu
Rolls Royce Corp.
Indianapolis, Indiana
US

ABSTRACT

Deposit formation on turbine hardware in propulsion turbine engines can occur in many arid regions globally. Characterising crystalline deposits on metallic substrates can aid in component resilience and health monitor algorithms during particle ingestion. This study has developed two statistical empirical models for prediction from acquired experimental data for the onset of deposits. The prediction models are for crystalline particulate (Arizona Road Test Dust) deposits on a flat rectangular Hastelloy-X test coupon. Particle impingement angles varied between 20° and 80° in experimental flow temperatures of 1,000–1,100°C. Averaged deposits are methodically quantified through normalised particle deposit tallies per area and percent coverage of the surface using microscopic imaging and image processing programs. Deposit accumulation is a quadratic function of both near-surface coupon temperature and coupon angle.

Keywords: Sand; deposition; turbines; Arizona Road Dust

Received 31 October 2016; revised 24 April 2017; accepted 3 April 2017; first published online 21 June 2017.
This paper will be presented at the ISABE 2017 Conference, 3-8 September 2017, Manchester, UK.

NOMENCLATURE

ARD	Arizona Road Dust
CCD	Central Composite Design
VTAR	Virginia Tech Aerothermal Rig

Symbols

D_P	average particle deposits per area
D_{CA}	average percent coverage area
R^2	coefficient of determination
R^2_{adj}	adjusted coefficient of determination
T_{NS}	near-surface coupon temperature
θ	coupon angle (degrees)

1.0 INTRODUCTION

Propulsion turbine engine particulate ingestion is a common issue in many arid regions. Typically, ingested sand and dust can produce glassy deposits on combustor and turbine components, which can cause detrimental effects ranging from reduced performance to complete engine failure. Characterising deposits depends on a variety of conditions, such as the mass ingested, particulate constituents, turbine component materials and operating conditions. There are a variety of methods to combat detrimental effects including reducing engine power during an ingestion event or increasing the service interval frequency for the exposed turbine engines. However, during extreme dust ingestion conditions, catastrophic engine failure is possible. This study provides results from analysis of data from a conducted experiment involving the initial deposits of crystalline particulate, Arizona Road Dust (ARD), on a flat rectangular Hastelloy-X test coupon as a relative analogue to actual turbine components. The data from the experiment is aggregated and analysed through two statistical empirical models for prediction.

Prominent examples of partial and complete turbine engine failure in airframes and equipment have been documented for several decades. For instance, during the Mount St. Helens eruption, an L-100 aircraft had two engines fail while the other two had partial power loss while flying below the ash cloud after the eruption began[(1)]. On 17 May 2015, a US Marine MV–22 Osprey had a fatal crash during a training exercise in dusty conditions while performing a hover manoeuvre. The right engine flamed out, causing the craft to drop 26 meters to the ground. Two US Marines were killed in the event with the remaining crew sustaining mild to severe injuries[(2)]. The post-accident report cited glassy deposits on the turbine section components as one of the direct causes of the engine failure.

Ingested particulate can be separated into two general categories, crystalline and amorphous. Crystalline particles, henceforth referred to as sand, are commonly found in desert regions whereas amorphous particles are found in volcanic ash. Since sand can vary in composition and size, previous airframe testing determined the quantity and sizing of lofted sand in brownout conditions[(3)]. Typical lofted sand concentrations in extreme rotor wash conditions (depending on airframe) can be as high as 0.005 kg-sand per kg-air. In addition, sand composition can vary depending on geographic location. For instance, even in a relatively

https://doi.org/10.1017/aer.2017.48 Published online by Cambridge University Press

small region in the Dhahran area, the composition of sand is primarily SiO_2 and Al_2O_3 but can vary in large proportions[4,5]. The large variation in sand composition will affect the deposit formation and accumulation[6].

Crystalline material phase structure and motion mechanisms relative to temperature can determine the probability that a particle will stick to a substrate. Since sand is composed of a variety of base constituents, the response of each non-homogenous material can vary at high temperatures. Generally, particulate material proceeds through four structure phases as temperature increases through the sintering process. They are designated as the shrinking, deformation, hemisphere and flow phases[7]. Each phase temperature can vary depending on the particulate constituents. In the context of turbine engine deposits, as the combustion temperatures increase, the particulate effectively softens or liquefies, which increases the probability of deposits onto a turbine component substrate. Particulate motion mechanisms associated with deposition are inertial impaction, turbulent diffusion/eddy impaction, Brownian diffusion, and thermophoresis[8]. Previous testing and modelling has demonstrated deposits as a function of particulate sizing. Stokes number is usually able to characterise the likelihood of a particle trajectory before impacting a substrate using the particle size. For Stokes numbers greater than unity, which are typically larger than one micron, the particulate is more likely to be dominated by inertial effects and resist changing direction due to the flow field. Since this study utilises 20–40 μm ARD, the primary mechanism is inertial impaction for all test conditions.

2.0 EXPERIMENT METHOD

All test were performed using the Virginia Tech Aerothermal Rig (VTAR) at the Advanced Propulsion and Power Laboratory at Virginia Tech. VTAR is capable of an 1,100°C maximum flow temperature at the test section for various sand injection concentrations. Tests were conducted at flow temperatures between 1,000°C and 1,100°C with coupon angles of 20°, 50° and 80°. The experimental design is a Central Composite Design (CCD) with repeated central tests[9]. The deposition data produced two empirical models for prediction as a function of near-surface coupon temperature and coupon angle.

2.1 Virginia Tech Aerothermal Rig

VTAR was donated by Rolls-Royce (Indianapolis, Indiana) to Virginia Tech in 2010. The previous application prior to the donation was heat transfer studies of cascade turbine aerofoils[10–13]. The test equipment was repurposed for high-temperature particle tracking studies by quantifying the coefficient of restitution[14,15]. The most recent study was for ARD deposit accumulation for very high sand loading and concentrations[16].

Figure 1 is a rendering of VTAR's current configuration for sand deposition testing. Propane is the fuel source for the sudden expansion burner. The total air flow rate leaving the burner is about 0.06 kg/s depending on the flow temperature. The equilibration tube is constructed of stainless steel alloy 310 with an inner diameter of 7.62 cm. The distance from the sand injector point to the end of the equilibration tube inside the test section is about 2.22 m. The equilibration tube length allows a sufficient amount of time for the temperature of the sand particles to equalise with the flow temperature. The injector inside the equilibration tube is directed upstream to promote sufficient mixing. A constant flow velocity leaving the equilibration tube is 70 ±2 m/s for all tests in this study to maintain consistency from the

https://doi.org/10.1017/aer.2017.48 Published online by Cambridge University Press

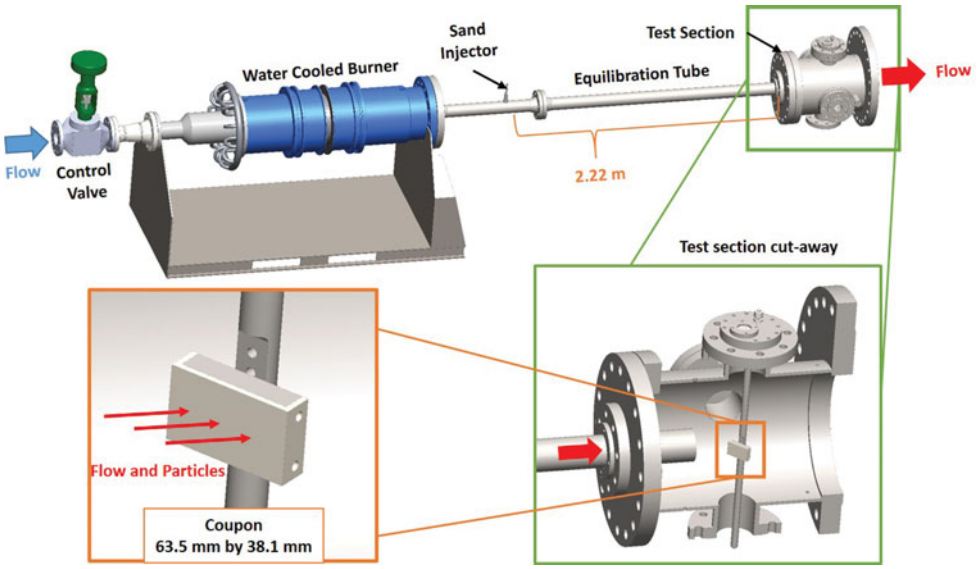

Figure 1. (Colour online) The Virginia Tech Aerothermal Rig (VTAR) utilised for deposition testing between 1,000°C and 1,100°C, highlighting the test section cut-away view and the associated coupon.

previous studies using VTAR[14–16]. The maximum flow temperature that can be achieved at the coupon is 1,100°C.

The test sand is dried in an oven at 120°C for a minimum of 12 hours prior to a test. Most excess water trapped in the particulate evaporates, which prevents "clumping" during the injection process. Dry ARD is entrained in a flow separate from the main flow using a conveyor-Venturi injection system. Sand is placed on a conveyor belt inside a sealed box to prevent contamination from environmental dust and humidity levels. The conveyor belt moves and drops the sand into Venturi vacuum pump. A conveyor scraper is used to passively ensure a majority of the sand drops into the pump. From system testing, mass losses are less than 0.01 g from the conveyor into the vacuum Venturi pump. To equalise the pressure inside the box due to the Venturi vacuum pump, a particulate filter and an air drying system ensures that the local environmental humidity does not alter the sand consistency during testing. Secondary containment around the conveyor belt reduces potential agitation of the sand due to air movement in the primary containment box. After the sand moves through the Venturi vacuum pump, the sand-laden flow travels through a hose that is attached to the injector nozzle on the equilibration tube.

The coupon angle illustrated in Fig. 2 (left) is the acute angle between the flow and the surface of the coupon where 0° is parallel and 90° is perpendicular to the flow. The coupon can be rotated in 10° increments along the vertical axis of the test section. Flow temperature is measured with three K-type thermocouples placed along the horizontal midline next to the coupon leading edge as well as above and below the coupon while being centred horizontally, illustrated in Fig. 2 (right). Due to the size and angle of the coupon relative to the equilibration tube, all the thermocouples are within the gas path. Two K-type thermocouples are placed directly behind the coupon to measure near-surface coupon temperature. The distance from the end of the equilibration tube to the leading edge of the coupon is approximately 10 cm. The distance decreases by about 2–3 cm during operations due to the thermal expansion of

https://doi.org/10.1017/aer.2017.48 Published online by Cambridge University Press

Table 1
Constant test conditions for varying flow temperature and coupon angle testing

Bulk Flow Velocity	**70 ±2 m/s**
Desired Gas Path Temperature Range	1,000°C, 1,050°C and 1,100°C
Particulate Type/Size	ARD, 20–40 μm
Injection Rate	0.0570–0.0646 g/s
Total Sand Loading	10 ±0.005 g
Coupon Angles	20°, 50° and 80°
Coupon Material	Hastelloy X
Coupon Surface Roughness	≤0.2 μm Root Mean Square
Coupon Thickness	3.175 mm
Particle Stokes Number	∼1.6 (20 μm) to 6.8 (40 μm)

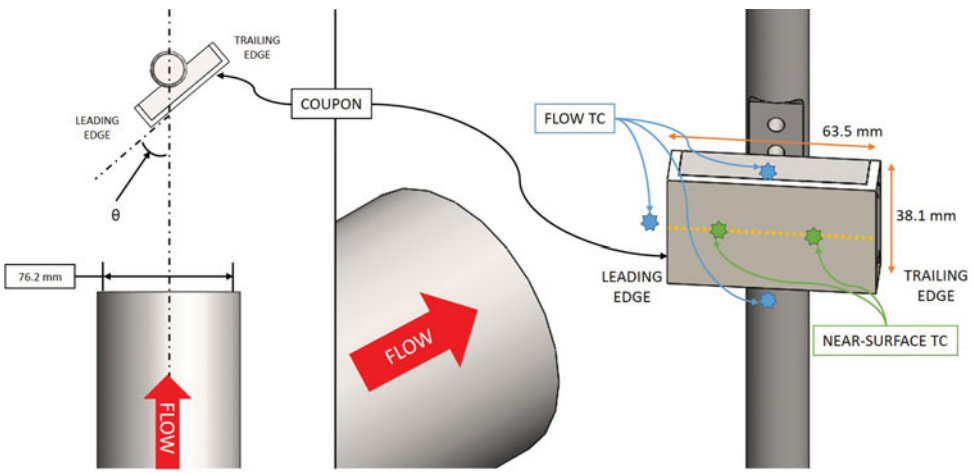

Figure 2. (Colour online) Two views of the coupon arrangement. Left: top-down view of coupon and equilibration tube with the test section casing and flanges hidden. The coupon angle, θ, is the acute angle between the bulk flow and the coupon surface. Right: an isometric view of the coupon and equilibration tube indicating thermocouple placement top and bottom of the coupon. The yellow dashed line across the coupon surface indicates the horizontal midline of the coupon and gas flow path.

the tube into the test section via a slip joint. Hastelloy-X is the coupon material, which is the same as in previous studies[14–16].

2.2 Experiment testing conditions

Independent variables (or predictors) for this study are bulk flow temperature and coupon angle. Deposited particles per area and percentage of coverage on the coupon surface by the deposits are the dependent variables. Table 1 provides a summary of the experiment test conditions. Flow temperature during injection is maintained within 5°C of the target

https://doi.org/10.1017/aer.2017.48 Published online by Cambridge University Press

temperature, which is 1,000°C, 1,050°C or 1,100°C. Near-surface coupon temperatures are measured for the subsequent statistical model (see Fig. 2). The near-surface and surface temperatures of the coupon vary depending on the coupon angle (20°, 50° or 80°) due to various heat transfer mechanisms during testing inside the test section. Only 10 ±0.005 g of ARD are used per test. The coupon is composed of Hastelloy-X and is polished to a mirror-like finish before each test with a measured root mean square roughness of less than 0.2 μm to ensure surface roughness effects are minimised for deposition.

The 20–40 μm ARD batch used in all tests is ISO test dust grade from Powder Technologies Inc. The Stokes number for the experiment is 1.6–6.8 depending on local velocity near the coupon surface. The mean diameter of the ARD is 26.58 μm with a median diameter of 27.3 μm. About 90% of the sand volume is between 20 and 40 μm, with the remaining 10% being less than 20 μm. Silicon and aluminium oxides are the primary constituents of ARD. An earlier study determined that ARD has a sintering temperature (shrinking phase) of 1,100°C for sizing less than 63 μm. Since the ARD is in a softened state, the sand particles may adhere to the Hastelloy-X surface[17]. The authors are aware that ARD is not an accurate analogue of airborne sands and dusts found across the world[18]. In addition, the particles typically entering the hot section of a turbine engine have a mean diameter less than 10 μm[19]. However, the ARD sizing used for this study improves the detection of deposited particles for post-test image processing and analysis as well as allowing a comparison to previous and potentially future deposition studies at Virginia Tech[14–16].

VTAR's sand injection system has been updated from the previous microparticle rebound and deposition studies[14–16] to allow for precise injection rate control that would be similar to turbine engine dust ingestion conditions. Dust concentrations ingested by turbine engines can be as high as 0.005 kg sand per kg air for extreme low-visibility conditions[3]. Injection rates for this study are 0.057–0.0646 g/s for approximately three minutes, which correlates to about 0.001 kg sand per kg air. Sand concentration variation is directly correlated to the variation in mass flow rate per test through the burner. Based on the operational parameters of VTAR, to maintain the velocity at 70 m/s as temperature increases, the mass flow rate must decrease. Regardless of the mass flow rate of the gas path and the associated concentration, the equilibration tube allows the particles to attain thermal and momentum equilibrium with the main flow before impacting or being diverted around the coupon.

For each test, VTAR is brought up to steady-state flow conditions at the appropriate flow temperature and velocity. Flow temperature is set by the maximum temperature associated with each test angle (Fig. 2). For instance, at angles of 20° and 50°, the maximum temperature is the leading-edge temperature. However, at 80°, the maximum temperatures are on the top and bottom of the coupon. Since the flow is being deflected around the coupon, there are recirculation zones on the trailing and leading edges, which lower the measured temperature at those locations. Due to the variation in flow temperature measurement locations and heat transfer mechanisms inside the test section, the primary variable compared to deposits is the average near-surface coupon temperature (Fig. 2). Experimental relationships for jet impingement onto a flat plate[20] determined the heat transfer coefficients to estimate coupon surface temperatures for each test angle. Using the heat transfer coefficient and estimating the radiative heat transfer, the variation of temperature between the surface and near-surface is less than 5°C depending on coupon angle for the experimental setup. Therefore, near-surface temperature is used as an independent variable for the empirical modelling.

ARD deposit accumulation on the inner walls of the equilibration tube is negligible for all testing. Periodic borescope inspections of the equilibration tube indicate minimal deposit accumulation. Regardless, molten sand particles may adhere to the inside of the stainless

https://doi.org/10.1017/aer.2017.48 Published online by Cambridge University Press

steel equilibration tube during testing. However, during the cool-down process after each test, any deposited material most likely delaminated from the equilibration tube and carried downstream. Since the equilibration tube has minimal deposits between tests, one test result should not affect a subsequent tests. Future studies will be necessary to accurately quantify any deposits that may occur on parallel flow surfaces using ARD.

2.3 Statistical modelling method

A multiple linear regression model is developed for estimating initial ARD deposits at various coupon angles and near-surface temperatures. There are a total of nine possible test combinations for flow temperature and angle. Primary control factors are the flow temperatures set at 1,000°C, 1,050°C and 1,100°C and three coupon angles set at 20°, 50° and 80°. A central composite design (CCD) is the most popularly used experimental design for fitting a second-order response surface[9]. A CCD is composed of factorial points for all possible high and low combinations of the factors, centre points which provide information about curvature of the response surface, and axial points which allow for estimation of quadratic effects. Since there are two factors with three levels each, a cuboidal CCD assists with studying curvature effects of the responses. With a minimum of nine possible combinations, three additional tests are performed at the centre levels for coupon angle (50°) and flow temperature (1,050°C) to ensure repeatability and curvature effects. By comparison, the CCD in this study uses 12 total tests, while a full factorial design with test triplication would require a minimum of 27 tests. The results from the CCD can be used for efficient estimation of first and second-order terms of the response surface of interest.

The fully randomised test order for the CCD is generated by JMP. Randomising the order of the experimental trials reduces bias caused by nuisance factors, such as equipment warm-up effects and daily atmospheric conditions. Each ARD sample is also randomly assigned to each experimental test condition.

3.0 RESULTS AND ANALYSIS

Deposits are quantified through microscopic images and processed to identify the normalised particle deposit tallies per square millimetre and percent coverage of the Hastelloy-X coupon surface. Deposits from both metrics are identified automatically and manually validated for each acquired image. The deposit data is averaged per test and combined to create two statistical empirical models. Heavy particle overlapping is observed for flow temperatures above 1,050°C and 50° coupon angle.

3.1 Data acquisition and reduction

Figure 3 (left) is a comparison example of the coupon surface at 20× magnification before and after each test at 1,050°C at 50°. Each microscopic image is the about 698 μm by 522 μm. Deposits metrics are average particles per area (particles per square millimetre) and average percent coverage. Quantifying the total deposits on the coupon surface uses a similar to the earlier deposition study at Virginia Tech[16].

The microscope system available requires manual acquisition of each location on the coupon. Based on the coupon orientation in the test section, three sample image rows are acquired across the horizontal axis of the coupon. Figure 3 (right) shows the location of each image series, which are at one-quarter, one-half, and three-quarters the relative vertical distance of the coupon. Three sample image rows provide triplicate data sets for each test

https://doi.org/10.1017/aer.2017.48 Published online by Cambridge University Press

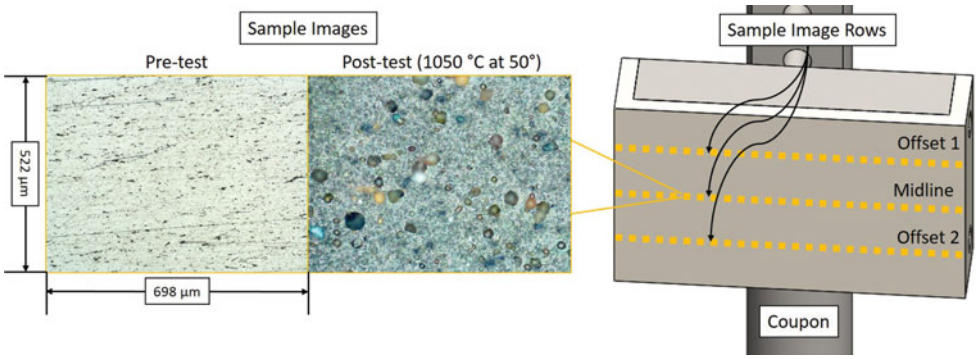

Figure 3. (Colour online) Left: pre-test and post-test surface sample image comparison showing the deposits and Hastelloy-X surface. The image size is 698 µm by 522 µm at 20× magnification. Right: rendered image of the coupon surface that highlights the locations of the sample image rows that are located at the midline, and the one-quarter and three-quarter locations vertically along the horizontal axis.

condition and validates the coupon exposure to the main gas path flow conditions. From each sample image row, approximately 50–60 images are acquired in relatively equal spacing for each cord across the surface from the leading edge towards the trailing edge. An exact location cannot be determined with manual acquisition, so equal spacing is assumed for all images across each series.

Each image is acquired with the focus set to the Hastelloy-X substrate, which causes the particle deposits to be slightly out of the focus plane resulting in a distinct boundary between the deposit and the heterogeneous surface pattern. Using the pattern and texture differences from the Hastelloy-X surface and deposits on the coupon surface, each image is processed using several functions from the MATLAB Visual Processing Toolbox. The image processing script is able to automatically identify most deposit particles and regions larger than 10 µm across for each image. Particle deposits less than 10 µm in diameter are disregarded based on the size distribution of the ARD supplied for this study. After the automatic selection process, each image is manually checked for incorrect identification and corrected if necessary. The combination of automatic and manual identification is capable of low variability and high repeatability between analysts.

Delamination of the particles from the coupon after testing (during VTAR cool-down) and during image processing is not observed. The local bond between Hastelloy-X and SiO_2, a primary constituent of ARD, is a strong atomic-level bond that resists thermal cycles. Prior research has implied that a crystalline SiO_2 layer between a nickel-based alloy and a crystalline thermal barrier coating would provide the bond strength necessary to prevent delamination during thermal cycling[21].

3.2 Raw data

Table 2 is the testing order, near-surface temperatures and average deposit data for each test condition for all three sample image rows. As expected, deposits typically increase with increasing surface temperature and coupon angle.

Figure 4 correlates the deposit data with near-surface temperature and shows that the deposit trends increase with coupon angle. In addition, the 95% confidence intervals are plotted at each test result from the resulting deposit model discussed in the following section. The repeated tests at 1,050°C and 50° coupon angle show very little variation between the

https://doi.org/10.1017/aer.2017.48 Published online by Cambridge University Press

Table 2
Aggregated deposit data for each test as well as the average near-surface temperature

Flow Temperature (°C)	Coupon Angle (°)	Average Near-Surface Temperature (°C)	Average Particles per mm^2	Average Percent Coverage
1,000	20	877	6	0.342
1,000	50	879	13	0.806
1,000	80	867	37	1.43
1,050	20	911	49	2.20
1,050	50	917	210	7.44
1,050	50	917	167	6.27
1,050	50	917	172	6.61
1,050	50	916	155	6.84
1,050	80	898	193	8.48
1,100	20	951	139	6.63
1,100	50	966	364	24.5
1,100	80	934	335	21.9

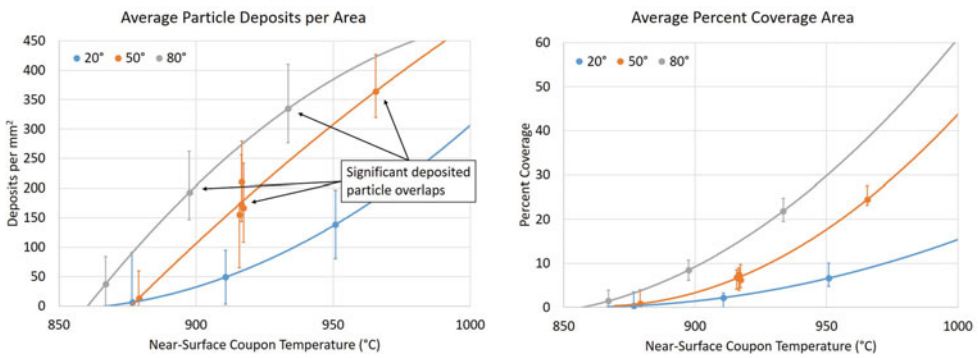

Figure 4. (Colour online) Left: average particle deposits per square millimetre on the coupon, and (right) average deposit percent coverage area on the coupon. Both responses are plotted against near-surface coupon temperature. The average deposits per square millimetre is less than anticipated due to significant deposited particles overlapping on the surface. The 95% confidence intervals are shown for each test case.

four tests for both deposits per square millimetre and percent coverage area. Comparing the raw deposit data for particle deposits per square millimetre and percent coverage area, the maximum total deposits observed occurs at 1,050°C flow temperature at 80° coupon angle. Near-surface temperatures at 80° coupon angle are lower than their counterparts at 20° and 50°. Convective recirculation area behind the coupon and radiative heat transfer mechanisms result in lower observed substrate temperatures. Specifically, at 80° coupon angle, there is a large stagnation region that develops in front of the coupon. The stagnation region can cause a large portions of the particles to be diverted around the coupon or decrease in velocity where they will not deposit. Reduced deposits at high angles and high temperatures have been

https://doi.org/10.1017/aer.2017.48 Published online by Cambridge University Press

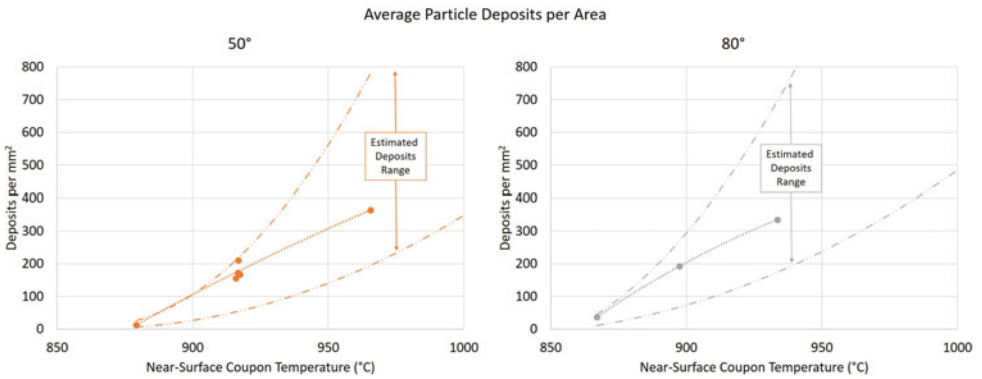

Figure 5. (Colour online) Particle deposits per area for the 50° and 80° coupon angle test cases with an estimated interval using the coverage area data.

observed before for a previous study at Virginia Tech that evaluated deposits under very high particulate loading at 1,100°C and 90° coupon angle[16].

Despite the underestimated particle deposits per area, a deposit-per-area estimated range is calculated using the percent coverage area data as seen in Fig. 5. Average deposits per square millimetre increase linearly while the percent coverage area increases at a quadratic rate. Deposits greater than 1,050°C flow temperatures and at 50° coupon angles show significant particle overlaps and large deposit regions. Overlapping particles are relatively indistinguishable for the image processing scripts and manual validation, which implies particle counts per image are underestimated at higher surface temperatures and coupon angles. Assuming the maximum and minimum size of a potential particle deposit has a diameter of 20–40 μm, the lower and upper bounds are calculated. Particle deposits per square millimetre are within the estimated boundaries but the raw data rate of increase does not correlate to the estimated boundary rates. For this study, both average particle deposit and percent coverage area data indicate the necessity to use a combination of empirical models to predict the onset of deposits.

3.3 Empirical models for prediction

Average deposits per area and percent coverage area are the primary dependent variables for both statistical empirical models for prediction. The near-surface temperature and coupon angle are the predictors (or independent variables) for average deposits per area and percent coverage. Near-surface temperature is converted from Celsius to Kelvin for an absolute temperature scale. JMP and MATLAB statistical modelling results are compared and validated for the empirical prediction models. All predictors included in the models presented are statistically significant at the 0.05 level of significance. This implies that predictors in the final models are useful in predicting average deposits per area and percent coverage.

The empirical model for average particle deposits per square millimetre Equation (1) has a strong correlation with both near-surface temperature and coupon angle predictors. The deposits-per-area empirical model contains an interaction between near-surface temperature and coupon angle. This means that the effect of near-surface temperature on the average particle deposits per square millimetre depends on the coupon angle. The coefficient of determination and adjusted coefficient of determination, R^2 and R^2_{adj}, respectively, are greater

https://doi.org/10.1017/aer.2017.48 Published online by Cambridge University Press

Table 3
R-squared and adjusted R-squared values for particle deposits per area for Equation (1) and deposit percent coverage Equation (2)

	Particle Deposits per Area	Deposit Percent Coverage
R^2	0.973	0.994
R^2_{adj}	0.963	0.989

than 90% (Table 3). The R^2 value is a measure of how well the empirical model approximates the deposit data points. A R^2 value of 1.0 means that the model fits the data perfectly. By contrast, the R^2_{adj} value accounts for the number of predictor variables and polynomial order within the model. For example, if there are too many predictors and/or higher-order polynomials, random noise can be unintentionally modelled. Therefore, the R^2_{adj} value can assist in avoiding overfitting an empirical model for prediction.

$$D_p = -4179.2 + 3.5266\ T_{NS} + 3.132\ \theta + 0.045799\ (T_{NS} - 1185.4)\,(\theta - 50) \quad \ldots(1)$$

The average deposit percent coverage empirical model Equation (2) has a stronger correlation for the near-surface temperature and coupon angle predictors compared to the Equation (1) model. The percent coverage model uses second-order predictors for near-surface temperature and coupon angle. Second-order predictors are necessary to achieve high R^2 and R^2_{adj} values as shown in Table 3. A quadratic response correlates with the average percent coverage trends in Fig. 4. By comparison, the deposits-per-area data in Fig. 4 are relatively linear for the 50° and 80° cases, which will overpower the quadratic response of the 20° tests. As mentioned in previously in Section 3.2, there is significant deposit overlapping for the higher coupon angles and temperatures that results in underestimation. Therefore, the percent coverage area prediction model is more representative of deposits compared to the deposits-per-area model at higher temperatures.

$$\begin{aligned} D_{CA} = {} & -269.63 + 0.22378\ T_{NS} + 0.20534\ \theta + 0.004718\ (T_{NS} - 1185.4)\,(\theta - 50) \\ & + 0.0021594\ (T_{NS} - 1185.4)^2 + 0.0014217\ (\theta - 50)^2 \end{aligned} \quad \ldots(2)$$

4.0 CONCLUSION

This study developed two statistical prediction models with experimental data for the onset of ARD sand deposits on a flat Hastelloy-X coupon at high temperatures as quadratic functions of near-surface coupon temperature and coupon angle. Flow temperatures are between 1,000°C and 1,100°C at 70 m/s, ARD is injected between 0.0570 and 0.0646 g/s, and coupon angles are set at 20°, 50° and 80°. Deposit accumulation between 1,050°C and 1,100°C flow temperatures for coupon angles greater than 50° has significant particle deposit overlapping. High levels of particle deposit overlap result in an underestimating prediction model (Equation (1)) at about 1,050°C. An average percent coverage area prediction model (Equation (2)) is able to quantify deposit accumulation despite the high levels of particle overlap. Therefore, a combination of Equations (1) and (2) is necessary to estimate surface deposits. In addition, particle deposit overlap and high substrate percent coverage indicates

https://doi.org/10.1017/aer.2017.48 Published online by Cambridge University Press

a shift towards utilising alternative data processing and prediction models. Using mass or surface roughness analysis of a test specimen is a subsequent data acquisition method that has been used in other studies to establish a way of estimating deposit accumulation.

This experiment can be expanded for future test scenarios. For instance, future experiments may involve particle tracking to characterise deposits as a function of near-surface temperature and particle impact vectors. In addition, altering coupon temperature as an analogue to turbine cooled hardware can expand the current statistical model.

ACKNOWLEDGEMENTS

The work presented here was supported by Rolls-Royce Plc., especially Brett Barker, Dr. Kwen Hsu and Paul Davis as well as Virginia Tech's Laboratory for Interdisciplinary Statistical Analysis (LISA).

REFERENCES

1. GABBARD, C.B., LELEVIER, R.E. and PARRY, J.F.W. Dust-Cloud Effects on Aircraft Engines—Emerging Issues and New Damage Mechanisms, Defense Technical Information Archive, 1982, Defense Nuclear Agency, Washington, D.C., US.
2. WHITTLE, R. "Fatal Crash Prompts Marines to Change Osprey Flight Rules," Breaking Defense, available at http://breakingdefense.com/2015/07/fatal-crash-prompts-marines-to-change-osprey-flight-rules/(accessed 15 August 2016, 16 July 2015.
3. COWHERD, C. Sandblaster 2 Support of See-Through Technologies for Particulate Brownout Task 5 Final Technical Report, Report No. 110565.1.005, 2007, U.S. Army Aviation and Missile Command, Arlington, Virginia, US.
4. SMIALEK, J.L. The Chemistry of Saudi Arabian Sand—A Deposition Problem on Helicopter Turbine Airfoils, NASA TM-105234, 1991, NASA, Cleveland, Ohio, US.
5. SMIALEK, J.L., ARCHER, F.A. and GARLICK, R.G. Turbine airfoil degradation in the Persian Gulf war, *J Minerals, Metals & Materials Society*, 1994, **46**, (12), pp 39-41.
6. KIM, J., DUNN, M.G. and BARAN, A.J. The "Most Probable" Dust Blend and Its Response in the F-100 Hot Section Test System (HSTS), DNA-TR-91-160, 1992, Defense Nuclear Agency, Alexandria, Virginia, US.
7. SONG, W., HESS, K.-U., DAMBY, D.E., WADSWORTH, F.B., LAVALLÉE, Y., CIMARELLI, C. and DINGWELL, D.B. Fusion characteristics of volcanic ash relevant to aviation hazards, *Geophysical Research Letters*, 2014, **41**, (7), pp 2326-2333.
8. HAMED, A., TABAKOFF, W.C. and WENGLARZ, R.A. Erosion and deposition in turbomachinery, *J Propulsion Power*, 2006, **22**, (2), pp 350-360.
9. MYERS, R.H., MONTGOMERY, D.C. and ANDERSON-COOK, C.M. *Response Surface Methodology: Process and Product Optimization Using Designed Experiments*, 2009, Wiley, Hoboken, New Jersey, US.
10. TURNER, E.R., WILSON, W.D., HYLTON, L.D. and KAUFMAN, R.M. Turbine Vane External Heat Transfer, Volume 1. Analytical and Experimental Evaluation of Surface Heat Transfer Distributions with Leading Edge Showerhead Film Cooling, NASA CR-174827, 1985, Indianapolis, Indiana, US.
11. HYLTON, L.D., NIRMALAN, V., SULTANIAN, B.K. and KAUFMAN, R.M. The Effects of Leading Edge and Downstream Turbine Vane Heat Transfer, CR-182133, 1988, NASA, Washington, D.C., US.
12. NEALY, D.A., MIHELC, M.S., HYLTON, L.D. and GLADDEN, H.J. Measurements of heat transfer distribution over the surfaces of highly loaded turbine nozzle guide vanes, *J Engineering for Gas Turbines and Power*, 1983, **106**, (January 1984), pp 149-158.
13. HYLTON, L.D., MIHELC, M.S., TURNER, E.R., NEALY, D.A. and YORK, R.E. Analytical and Experimental Evaluation of the Heat Transfer Distribution over the Surfaces of Turbine Vanes, CR-168015, 1983, NASA, Washington, D.C., US.

https://doi.org/10.1017/aer.2017.48 Published online by Cambridge University Press

14. DELIMONT, J.M., MURDOCK, M.K., NG, W.F. and EKKAD, S.V. Effect of temperature on microparticle rebound characteristics at constant impact velocity—Part II, *J Engineering for Gas Turbines and Power*, 2015, **137**, (11), p 112604.
15. DELIMONT, J.M., MURDOCK, M.K., NG, W.F. and EKKAD, S.V. Effect of temperature on microparticle rebound characteristics at constant impact velocity–Part I, *J Engineering for Gas Turbines and Power*, 2015, **137**, (11), p 112603.
16. BOULANGER, A.J., PATEL, H.D., HUTCHINSON, J., DESHONG, W., XU, W., NG, W.F. and EKKAD, S.V. Preliminary experimental investigation of initial onset of sand deposition in the turbine section of gas turbines, ASME Turbo Expo 2016, Volume 1: Aircraft Engine; Fans and Blowers; Marine, 2016, ASME, Seoul, South Korea, p. V001T01A003.
17. KUEPPERS, U., CIMARELLI, C., HESS, K.-U., TADDEUCCI, J., WADSWORTH, F.B. and DINGWELL, D.B. The thermal stability of Eyjafjallajökull ash versus turbine ingestion test sands, *J Applied Volcanology*, 2014, **3**, (1), p 4.
18. DUNN, M.G., PADOVA, C., MOLLER, J.E. and ADAMS, R.M. Performance deterioration of a turbofan and a turbojet engine upon exposure to a dust environment, *J Engineering for Gas Turbines and Power*, 1987, **109**, (3), p 336.
19. DUNN, M.G., PADOVA, C. and ADAMS, R.M. Operation of Gas Turbine Engines in Dust-Laden Environments, ADP006197, 1987, Buffalo, New York, US.
20. LIVINGOOD, J.N.B. and HRYCAK, P. Impingement heat transfer from turbulent air jets to flat plates: A literature survey, TM X-2778, 1973, NASA, Washington, D.C., US.
21. JARVIS, E.A.A. and CARTER, E.A. Exploiting covalency to enhance metal-oxide and oxide-oxide adhesion at heterogeneous interfaces, *J American Ceramic Society*, 2003, **86**, (3), pp 373-386.

https://doi.org/10.1017/aer.2017.48 Published online by Cambridge University Press